X-ray and neutron scattering study of Si-rich Si-Ge single crystals

D. Le Bolloc'h,[1,*] J. L. Robertson,[2] H. Reichert,[3] S. C. Moss,[1] and M. L. Crow[2]
[1]*Physics Department, University of Houston, Texas 77204-5504*
[2]*Solid State Division, Oak Ridge National Laboratory, Oak Ridge, Tennessee 37831*
[3]*Max-Planck-Institut für Metallforschung, D-70569 Stuttgart, Germany*
(Received 4 January 2000; published 2 January 2001)

The local atomic environments of homogeneous Si-rich Si-Ge single crystals were studied using x-ray and neutron diffuse scattering. No evidence of either chemical short-range order or clustering was observed. Static atomic displacements, however, were clearly present and are consistent with an expansion of the lattice in the vicinity of the Ge atoms. The dispersion of the acoustic phonons was also measured using inelastic neutron scattering. The acoustic modes of the Si-Ge alloy were found to lie nearer those of pure Si than expected from the homologous relationship found between pure Si and pure Ge.

DOI: 10.1103/PhysRevB.63.035204 PACS number(s): 61.82.Fk, 61.66.Dk, 63.20.−e, 61.43.−j

I. INTRODUCTION

In the past, the performance of devices based on silicon technology has been advanced primarily through component miniaturization. However, the limit where further reduction in size is no longer feasible for many applications is fast approaching. For this reason, future gains in performance depend upon either moving to other technologies such as Ga-As or developing silicon technology in new directions. One approach, which has already produced a considerable gain in performance, extends existing silicon technology by alloying silicon with germanium.[1] This has lead to the development of Si-rich Si-Ge alloys that are of great interest because the carrier mobility of the electrons and holes is much greater than that found in pure silicon.[2] Increased carrier mobility, along with other properties of Si-Ge alloys, is driving the development of new electronic devices with significantly improved operating frequency, power consumption, current density, and noise characteristics.[3,4]

Current applications of Si-Ge alloys generally rely upon thin-film technology, and a substantial literature exists on the structure[5–7] and physical properties[2,3,8,9] of such films. Various techniques are used to produce these films, mostly UHV/chemical vapor deposition[10] and molecular beam epitaxy,[11] and several strategies have been developed to enhance the desired properties (e.g., strain,[2,12,13] graded composition,[14] or self-assembled quantum dots[15]). For a more fundamental understanding of the Si-Ge alloy system, however, studies on equilibrium-phase bulk specimens are needed because the properties of thin films are often observed to differ from those of bulk materials. In this paper, we present preliminary results describing the local atomic environments and phonon dispersion of homogeneous $Si_{0.92}Ge_{0.08}$ and $Si_{0.9}Ge_{0.1}$ single crystals. To our knowledge, this is the first study of bulk Si-Ge single crystals with an excess of silicon.

II. SAMPLE PREPARATION AND CHARACTERIZATION

Although Si-Ge alloys have been available for more than ten years in the form of thin films, it has remained very difficult to grow homogeneous Si-Ge single crystals even though there is complete miscibility. Because of the large liquid/solid coexistence region and the large difference in the melting temperatures of the two components (1141 K for Si and 665 K for Ge), there is substantial constitutional supercooling relative to the congruent melting temperature of the alloy. Another difficulty encountered when using conventional crystal growth techniques to produce Si-rich Si-Ge single crystals is how to achieve a uniform distribution of the Ge atoms within the Si matrix. Recently, new crystal growth methods have been developed that can produce large $Si_{1-x}Ge_x$ single crystals with an exceptionally high degree of compositional uniformity.[16,17] The samples used in this study are homogeneous $Si_{0.92}Ge_{0.08}$ and $Si_{0.9}Ge_{0.1}$ single crystals that are free of dislocations and were prepared using the modified Czochralski technique described in Ref. 16. The $Si_{0.92}Ge_{0.08}$ crystal consisted of a little less than half of a 30-mm-diameter circular plate with a thickness of 2 mm for a total volume of $\sim 930\ mm^3$ and weighed 2.3 g. The $Si_{0.9}Ge_{0.1}$ crystal was a 0.1 g rectangular prism, roughly $17.5\,mm \times 5.2\,mm \times 0.5\,mm$, with a volume of $\sim 46\ mm^3$. The local composition of the crystal has been sampled at several positions using electron dispersive x-ray spectroscopy and no inhomogeneities were detected to within the accuracy of the technique up to a zone of 20 μm.

Characterization of the crystal using x-ray and neutron diffraction shows no evidence of any macroscopic variation in Ge content. No splitting of the Bragg diffraction profiles, which would result from the presence of a second phase, or peak broadening with increasing momentum transfer $|\mathbf{Q}| = 4\pi \sin(\Theta)/\lambda$, which would indicate long-range variation of the lattice parameter[18] in the same manner as strain broadening, was observed. The x-ray diffraction measurements probe the near-surface portion of the crystal, because of the shallow penetration depth, with high resolution, while the neutron diffraction measurements sample the entire volume of the bulk crystal. The mosaic spread of the crystal was determined to be 0.03°. Figure 1 shows transverse (rocking curve) and radial ($\Theta/2\Theta$) scans of the (200) Bragg peak using $0.709\,26\,\text{Å}\,(\text{Mo}\,K\alpha_1)$ x rays. The peak profiles of the Si-Ge alloy are compared with those of a perfect crystal of pure Si measured under identical conditions. The finite peak widths observed for the pure Si, crystal result from the resolution of

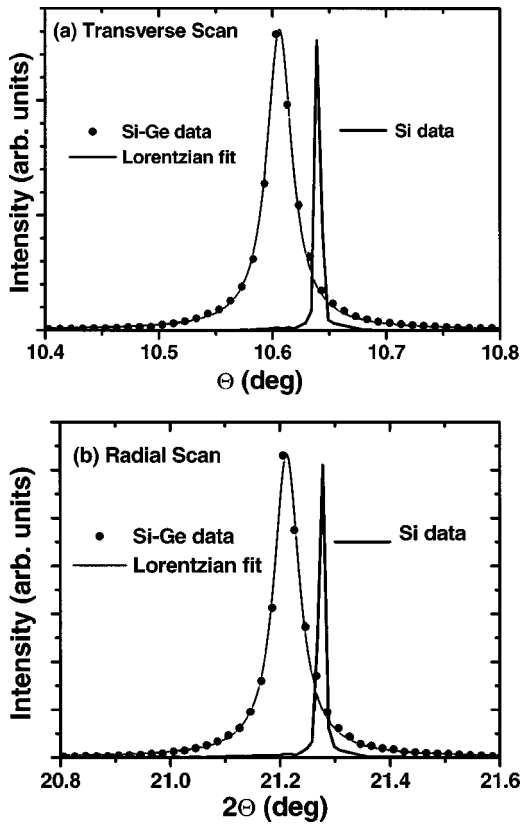

FIG. 1. Transverse (a) and radial (b) scans of the $Si_{0.92}Ge_{0.08}$ alloy. Each is compared to a corresponding scan on a wafer of pure Si, which is essentially the instrumental resolution.

the instrument. Both the transverse and radial peak widths of the Si-Ge alloy are about five times greater than the instrumental resolution. Crystals of this quality are quite acceptable for the experimental studies reported here.

III. LOCAL ATOMIC ENVIRONMENTS

Si and Ge both have the diamond cubic crystal structure and when alloyed form a continuous series of substitutional solid solutions over the entire composition range.[19] Thus the diamond cubic structure is preserved for all concentrations. Moreover, the Si and Ge lattice parameters differ by only ~4.2%, 5.430 54 Å for Si and 5.657 54 Å for Ge, and the lattice parameter of the alloy varies continuously with composition with a slight negative deviation from Vegard's law.[20] Previous studies of chemical short-range order in solid solutions have shown that at temperatures sufficiently below the melting point few, if any, are completely disordered. In other words, certain local atomic arrangements occur more often than one would expect from a completely random distribution of atomic species on the lattice. Several theoretical studies predict a miscibility gap in the Si-Ge system whose maximum occurs between $T=150$ K and 350 K.[21–24] These studies are supported by a previous study of a polycrystalline $Si_{0.5}Ge_{0.5}$ solid solution which showed a tendency toward phase segregation.[25] On the other hand, several long-range ordered structures have been reported in thin Si-Ge films although these were under either compressive or tensile strain.[26–28] And, finally, there is an x-ray absorption fine-structure (EXAFS) study of $Si_{1-x}Ge_x$ thin films that indicates that the alloy is indeed completely random.[29] Thus it was not at all clear at the outset whether the chemical short-range order in our bulk single crystals would favor ordering, clustering, or total randomness.

In general, the total coherent scattered intensity from a solid solution can be separated into two parts,

$$I_{\text{total}}(\mathbf{Q}) = I_{\text{Bragg}}(\mathbf{Q}) + I_{\text{diffuse}}(\mathbf{Q}), \tag{1}$$

where $\mathbf{Q}$ is the scattering vector, $I_{\text{Bragg}}(\mathbf{Q})$ is the scattering intensity containing information about the average lattice, and $I_{\text{diffuse}}(\mathbf{Q})$ is the scattering that arises from local deviations from the average structure. The average lattice is strongly correlated over thousands of angstroms and thus appears in the observed diffraction pattern as a series of narrow δ-like functions (convoluted with the instrumental resolution) located at the reciprocal lattice sites. By contrast, the diffuse scattering is weakly correlated over small distances, typically only a few unit cells, and so has very broad features that fill all of reciprocal space.

The diffuse intensity can be further divided into separate contributions from the various types of local deviation from the average structure:[30,31]

$$I_{\text{diffuse}}(\mathbf{Q}) = I_{\text{SRO}}(\mathbf{Q}) + I_{\text{SD}}(\mathbf{Q}) + I_{\text{TD}}(\mathbf{Q}), \tag{2}$$

where $I_{\text{SRO}}(\mathbf{Q})$ is the scattering arising from the local concentration fluctuations [short-range order (SRO)], $I_{\text{SD}}(\mathbf{Q})$ is the scattering from the static displacement (SD) field that dresses the concentration fluctuations, and $I_{\text{TD}}(\mathbf{Q})$ is the scattering arising from the dynamics of the system (thermal diffuse scattering from the phonons). During this part of the discussion we are mainly interested in $I_{\text{SRO}}(\mathbf{Q})$ and the first-order term in the static displacements. In the case of x-ray scattering from a cubic structure, $I_{\text{SRO}}(\mathbf{Q})$ is given by

$$I_{\text{SRO}}(\mathbf{Q}) = c_{\text{Si}}c_{\text{Ge}}|b_{\text{Si}} - b_{\text{Ge}}|^2 \sum_{lmn} e^{-2M\varphi_{lmn}}\alpha_{lmn} \times \cos(q_1 l + q_2 m + q_3 n), \tag{3}$$

and the first-order term of $I_{\text{SD}}(\mathbf{Q})$ is given by

$$I_{\text{SD}}(\mathbf{Q}) = c_{\text{Si}}c_{\text{Ge}}|b_{\text{Si}} - b_{\text{Ge}}|^2 \sum_{lmn} e^{-2M\varphi_{lmn}}(\mathbf{Q}\cdot\boldsymbol{\gamma}_{lmn}) \times \sin(q_1 l + q_2 m + q_3 n), \tag{4}$$

where c_{Si} and c_{Ge} are the concentrations of Si and Ge, respectively, b_{Si} and b_{Ge} are the neutron scattering lengths, and $e^{-2M\varphi_{lmn}}$ is the neighor-shell-dependent Debye-Waller factor. The indices l, m, and n denote the atomic coordinates of the neighboring atoms in units of the lattice parameter, i.e., the lattice vector $\mathbf{r}_{lmn}$ describing the relative position of a neighboring atom would be $\mathbf{r}_{lmn} = l\mathbf{a}_1 + m\mathbf{a}_2 + n\mathbf{a}_3$, where $\mathbf{a}_1$, $\mathbf{a}_2$, and $\mathbf{a}_3$ form the basis of the direct space lattice. Likewise, q_1, q_2, and q_3 are the reciprocal space coordinates defined by $\mathbf{Q} = q_1\mathbf{b}_1 + q_2\mathbf{b}_2 + q_3\mathbf{b}_3$, where $\mathbf{b}_1$, $\mathbf{b}_2$, and $\mathbf{b}_3$ are the reciprocal space basis vectors. These expressions apply equally well to x-ray scattering where one need only

replace the neutron scattering lengths b_{Si} and b_{Ge} with the corresponding x-ray atomic form factors f_{Si} and f_{Ge}. Finally, care must be taken when applying Eqs. (3) and (4) to diamond cubic structures because the primitive lattice contains two atoms per unit cell.

The α_{lmn}'s are the Warren-Cowley short-range order parameters and are the Fourier coefficients that describe correlations in the distribution of Si and Ge atoms on the lattice. These parameters have a direct physical interpretation:

$$\alpha_{lmn}=1-\frac{P_{lmn}^{\text{Si-Ge}}}{c_{\mathrm{Ge}}}=1-\frac{P_{lmn}^{\text{Ge-Si}}}{c_{\mathrm{Si}}}, \tag{5}$$

where $P_{lmn}^{\text{Si-Ge}}$ is the conditional probability of finding a Ge atom at position *lmn* given a Si atom at any origin site. So, for a perfectly random alloy where there are no correlations between site occupations, $\alpha_{000}=1$ (the probability of finding a Si atom on a site occupied by a Si atom) and all other α_{lmn}'s are zero. In this case, Eq. (3) reduces to

$$I_{\mathrm{SRO}}(\mathbf{Q})=c_{\mathrm{Si}}c_{\mathrm{Ge}}|b_{\mathrm{Si}}-b_{\mathrm{Ge}}|^2=I_{\mathrm{Laue}}(\mathbf{Q}), \tag{6}$$

also known as the Laue scattering. Surprisingly, this is what we observe. In both x-ray synchrotron measurements made on the $Si_{0.9}Ge_{0.1}$ crystal using beamline X-14 at the National Synchrotron Light Source located at Brookhaven National Laboratory and neutron diffuse scattering measurements made on the $Si_{0.91}Ge_{0.08}$ crystal using the HB3 triple-axis spectrometer at the High Flux Isotope Reactor (HFIR) located at Oak Ridge National Laboratory, no evidence of either clustering or ordering tendencies was observed. From Eq. (3) we see that the magnitude of $I_{\mathrm{SRO}}(\mathbf{Q})$ depends on the square of the scattering contrast, $|b_{\mathrm{Si}}-b_{\mathrm{Ge}}|^2$, as well as on the product of the concentrations. We can use these quantities to estimate the maximum amount of short-range order that could be present but unobservable, considering the statistical quality of the data and the regions of reciprocal space where the data were collected. Given that the probability of finding a Ge atom as the first neighbor of a Si atom is, in the case of a random alloy, just the concentration of Ge atoms, we conclude that the first-neighbor occupation probability $P_{\frac{1}{4}\frac{1}{4}\frac{1}{4}}^{\text{Si-Ge}}$ deviates from the Ge concentration by no more than 0.006 (0.6%) if the system were clustering or 0.002 (0.2%) if the alloy tended to order. Of course, the lack of chemical SRO could simply be due to the temperature from which the sample was necessarily quenched, even on slow cooling, since all predictions of phase separation occur near room temperature or, in our case, well below, and slow diffusion renders the achievement of the room-temperature equilibrium chemical short-range order impossible. The effective equilibrium temperature of the $Si_{0.92}Ge_{0.08}$ sample may be estimated from the cooling rate (slow cooled at ~25 K/min) and the diffusion of Ge in Si to be ~920 K, which is several hundred Kelvins above the predicted miscibility gap.

The absence of chemical short-range order does not, however, imply that no diffuse scattering was present. In both the x-ray and neutron measurements, we observed moderately intense scattering associated with the static displacements. This is not surprising since the lattice will still be expanded relative to the average lattice spacing in the vicinity of the larger atoms and contracted around the smaller atoms. The contribution from $I_{\mathrm{SD}}(\mathbf{Q})$ is distinguished from $I_{\mathrm{Bragg}}(\mathbf{Q})$ because it does not occur only at reciprocal lattice points, and from $I_{\mathrm{SRO}}(\mathbf{Q})$ because it has odd rather than even symmetry [see Eqs. (3) and (4)] relative to the center of the Brillouin zones (i.e., the Bragg peak positions). The contribution from $I_{\mathrm{TD}}(\mathbf{Q})$ was suppressed by cooling the sample to 20 K for the x-ray synchrotron measurements and eliminated for the elastic neutron measurement by using the energy analysis capability of the triple-axis spectrometer. In addition, the first-order term in the static displacements can be identified because it scales linearly with increasing $|\mathbf{Q}|$. The magnitude of the displacements is assumed to be small because the alloy is substitutionally disordered and the lattice parameters of the pure elements differ by only 4.2%. Thus only the first-order term of $I_{\mathrm{SD}}(\mathbf{Q})$ need be considered initially because the higher-order terms have a quadratic or greater dependence on the magnitude of the displacements and can therefore be neglected for the moment. The linear displacement parameters $\boldsymbol{\gamma}_{lmn}$ in Eq. (4) are related to the individual static displacements by

$$\begin{aligned}\boldsymbol{\gamma}_{lmn}=&\left(\frac{b_{\mathrm{Ge}}}{b_{\mathrm{Si}}-b_{\mathrm{Ge}}}\right)\left(\frac{c_{\mathrm{Ge}}}{c_{\mathrm{Si}}}+\alpha_{lmn}\right)\langle\boldsymbol{\Delta}_{lmn}^{\text{Ge-Ge}}\rangle\\&-\left(\frac{b_{\mathrm{Si}}}{b_{\mathrm{Si}}-b_{\mathrm{Ge}}}\right)\left(\frac{c_{\mathrm{Si}}}{c_{\mathrm{Ge}}}+\alpha_{lmn}\right)\langle\boldsymbol{\Delta}_{lmn}^{\text{Si-Si}}\rangle,\end{aligned} \tag{7}$$

where $\langle\boldsymbol{\Delta}_{lmn}^{\text{Si-Si}}\rangle$ and $\langle\boldsymbol{\Delta}_{lmn}^{\text{Ge-Ge}}\rangle$ are the species-dependent average displacements between pairs of atoms. Note that it is the mean value of the individual Cartesian components of the displacement vectors that is recovered from the data refinement (i.e., $\langle\boldsymbol{\Delta}_{lmn}^{\text{Si-Si}}\rangle=\langle\boldsymbol{\Delta}_{lmn}^{\text{Si-Si}}\rangle_x+\langle\boldsymbol{\Delta}_{lmn}^{\text{Si-Si}}\rangle_y+\langle\boldsymbol{\Delta}_{lmn}^{\text{Si-Si}}\rangle_z$). In general, the components of the displacement vector for a particular neighbor shell are not independent due to symmetry[30] and thus the number of free parameters is reduced. In order to further reduce the number of parameters, the terms involving $\langle\boldsymbol{\Delta}_{lmn}^{\text{Si-Ge}}\rangle$ and $\langle\boldsymbol{\Delta}_{lmn}^{\text{Ge-Si}}\rangle$ have been eliminated from Eq. (7) using the constraint that the sum of all the mean displacements for each neighbor shell must be zero to preserve the symmetry of the average lattice.[31] These terms can be recovered using the following expression:

$$\begin{aligned}\langle\boldsymbol{\Delta}_{lmn}^{\text{Si-Ge}}\rangle=\langle\boldsymbol{\Delta}_{lmn}^{\text{Ge-Si}}\rangle=-\frac{1}{2}\Bigg\{&\left[\left(\frac{\alpha_{lmn}+c_{\mathrm{Ge}}/c_{\mathrm{Si}}}{1-\alpha_{lmn}}\right)\boldsymbol{\Delta}_{lmn}^{\text{Ge-Ge}}\right]\\&+\left[\left(\frac{\alpha_{lmn}+c_{\mathrm{Si}}/c_{\mathrm{Ge}}}{1-\alpha_{lmn}}\right)\boldsymbol{\Delta}_{lmn}^{\text{Si-Si}}\right]\Bigg\}.\end{aligned} \tag{8}$$

Figure 2 shows a radial scan through the (220) Bragg peak using elastic neutron scattering. The diffuse intensity is greater than $I_{\mathrm{Laue}}(\mathbf{Q})$, indicated by the dotted line, on the low-*H* side of the peak and is less than $I_{\mathrm{Laue}}(\mathbf{Q})$ on the high-*H* side. This is a clear signature of first-order displacement scattering where the lattice is expanded in the vicinity of the larger atomic species (Ge) with the larger scattering power ($b_{\mathrm{Ge}}=8.185$ fm and $b_{\mathrm{Si}}=4.149$ fm). Similar behavior is observed around other Bragg peak positions.

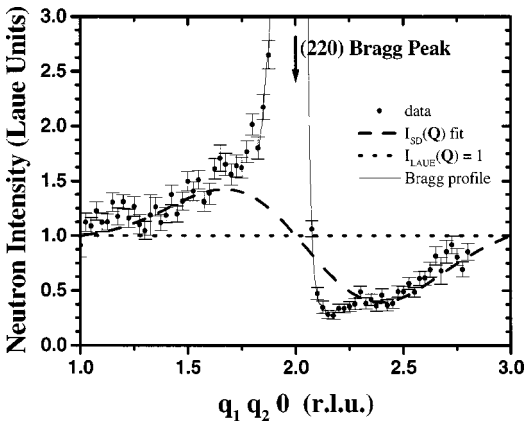

FIG. 2. Radial scan through the (220) Bragg peak using elastic neutron scattering. The solid circles with error bars show the normalized neutron intensity in Laue units. The small incoherent scattering was calculated and subtracted off during the normalization process. The dotted line indicates 1.0 Laue unit. The dashed line shows the results of a first- and second-neighbor fit to the first-order static displacements. The fact that the diffuse intensity goes from greater than the Laue scattering to less than the Laue scattering through the Bragg peak indicates that the lattice is expanded in the vicinity of the stronger scatterer—in this case, Ge. The thin solid line is the profile of the Bragg peak.

In order to obtain the individual displacements, diffuse intensity measurements over a large volume of reciprocal space using two different scattering contrasts are required. In the present case it is possible, in the absence of chemical short-range order scattering, to obtain the γ_{lmn}'s for the first few neighbor shells. The dashed curve in Fig. 2 shows the results of a least-squares fit to the first- and second-nearest neighbors, $\gamma_{\frac{1}{4}\frac{1}{4}\frac{1}{4}}$ and $\gamma_{\frac{1}{2}\frac{1}{2}0}$. Although the displacements for the first two neighbor shells are certainly much larger than those for more distant neighbor pairs, they are clearly insufficient to reproduce accurately the diffuse intensity. The inclusion of more parameters in the fit is not justified here due to the limited amount of data. It appears that inclusion of higher-order static displacement terms (e.g., Huang scattering) will also be needed. However, from this simple model, we can conclude that a positive value for both $\gamma_{\frac{1}{4}\frac{1}{4}\frac{1}{4}}$ and $\gamma_{\frac{1}{2}\frac{1}{2}0}$ is required. Due to the small Ge concentration the γ_{lmn}'s are dominated by $\langle \Delta_{lmn}^{\text{Si-Si}} \rangle$. From the fit in Fig. 2, we obtain a value of $|\gamma_{\frac{1}{4}\frac{1}{4}\frac{1}{4}}| = 1.2 \times 10^{-3}$ in units of the lattice parameter for the nearest-neighbor displacement parameter, which gives $|\langle \Delta_{\frac{1}{4}\frac{1}{4}\frac{1}{4}}^{\text{Si-Si}} \rangle| \approx -0.006$ Å assuming that the displacements are radial. This means that, on average, Si-Si first-neighbor pairs are compressed by 0.006 Å (0.25%) relative to the spacing of the average lattice. This value seems small compared to the displacements observed in metallic alloys with similar size ratios between the two atomic species.[32,33] This may be due in part to the open nature of the diamond cubic lattice with only four nearest neighbors as opposed to eight in the case of bcc and 12 for fcc structures.

Not much can be said at this point about $\langle \Delta_{\frac{1}{4}\frac{1}{4}\frac{1}{4}}^{\text{Ge-Ge}} \rangle$ and $\langle \Delta_{\frac{1}{4}\frac{1}{4}\frac{1}{4}}^{\text{Si-Ge}} \rangle$ without the full set of data needed to unravel the individual displacement contributions. Using the theory of Froyen and Herring,[34] we get

$$|\langle \Delta_{\frac{1}{4}\frac{1}{4}\frac{1}{4}}^{\text{Ge-Ge}} \rangle| = -\frac{c_{\text{Si}}}{c_{\text{Ge}}} |\langle \Delta_{\frac{1}{4}\frac{1}{4}\frac{1}{4}}^{\text{Si-Ge}} \rangle| = 0.054\ \text{Å}, \tag{9}$$

which indicates that most of the distortion of the lattice is in the vicinity of the Ge atoms, as expected for a dilute alloy. Caution must be used when applying Eq. (9) because the theory of Froyen-Herring has been shown to be invalid for systems where the displacements are primarily due to electronic structure effects rather than a large size mismatch between the atomic species.[32]

IV. PHONON DISPERSION

The phonon dispersion curves of pure Si and pure Ge are nearly homologous.[35–37] Using the perturbation expansion method, based on tight-binding electron wave functions in the Hartree-Fock approximation,[38] the vibrational energies β_{qj} of diamond cubic homopolar crystals can be transformed into a dimensionless form:

$$\Omega_{qj} = \frac{\beta_{qj}}{\hbar \sqrt{\mu a^3 / e^2}}, \tag{10}$$

where $\mu = m_1 m_2/(m_1 + m_2)$ is the reduced mass of the atoms, a is the lattice parameter, e is the charge on an electron, q is the phonon wave vector, and j is the phonon branch. If the phonon dispersion of a homopolar diamond cubic crystal is transformed using Eq. (10), the dimensionless energy Ω_{qj} becomes practically independent of the atomic species. This relationship has been demonstrated to hold true for Si, Ge, and gray Sn,[36] although a small difference between the dimensionless transverse acoustic branches of Si and Ge has been noted.[35]

The dispersion of the longitudinal and transverse acoustic phonons for the $Si_{0.92}Ge_{0.08}$ crystal in high-symmetry directions of the diamond cubic structure has been determined here using inelastic neutron scattering. The measurements were made on the HB2 and HB3 triple-axis spectrometers at the HFIR at ORNL. Both constant-energy transfer and constant-momentum transfer scans were made with a fixed final energy of $E_f = 14.7$ or 30.5 meV, depending on the focusing conditions and the position in reciprocal space where each scan was made. Pyrolytic graphite was used for both the monochromator and the analyzer on HB3 while a vertically focusing Be monochromator and a pryolytic graphite analyzer were used on HB2. Because of the small volume of the sample, the collimation was relaxed. For both HB2 and HB3 the effective collimation before the monochromator was 48′ and a 40′ collimator was used between the monochromator and the sample. On HB2 an 80′ collimator was used between the sample and the analyzer and a 120′ collimator between the analyzer and the detector. On HB3, 40′ and 70′ collimators, respectively, were used at these positions. Under these conditions the energy resolution was typically ~1 meV and was never greater than ~3 meV. In ad-

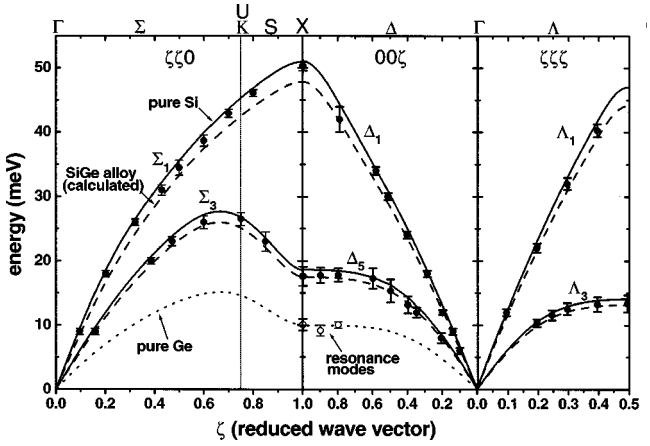

FIG. 3. Acoustic phonon dispersion of the $Si_{0.92}Ge_{0.08}$ alloy in the (110) plane. The high-symmetry directions, with the exception of the Σ_5 mode, are indicated by the solid circles. The dispersion of pure Si is given by the solid line and that of pure Ge by the dotted line. The dashed line shows the calculated dispersion of the alloy using Eq. (10). The open circles indicated resonance modes observed in the alloy.

dition, a 65-mm-thick pyrolytic graphite filter was used between the sample and the analyzer to suppress the higher-order contamination. The phonon measurements were made at room temperature in the (110) scattering plane so that the $\Delta=[001]$, $\Sigma=[110]$, and $\Lambda=[111]$ directions could be studied. The transverse acoustic mode Σ_3 could not be accessed in this geometry because the polarization is normal to the scattering plane.

Figure 3 shows the phonon dispersion of the $Si_{0.98}Ge_{0.08}$ alloy along with that of pure Si,[39] and pure Ge.[40,41] The observed phonon energies for the alloy are presented in Table I. The uncertainties in the position of the phonon groups from the constant-momentum transfer scans have been converted to uncertainties in the phonon energy using the slope of the dispersion and the calculated instrumental resolution. The individual phonon groups were unremarkable, except for a significant amount of broadening in energy of the Δ_1 branch at $\zeta=0.6$, due, perhaps, to interference with the resonance modes discussed below. The acoustic phonons in the alloy are found to be nearly homologous to those of the pure Si. From Eq. (10), the phonon energies of the Si-Ge alloy are expected to 6.2% lower than that of pure Si (see the dashed line in Fig. 2). However, the observed dispersion of the alloy is typically only 2– 3% less than that of pure Si and never more than 4.5% lower. Although the deviation from pure Si is greater along Δ_5 and appears to be more consistent with the expected homologous relationship, in reality this is expected from the observed behavior of this branch when Eq. (10) is applied to pure Si and Ge.[35] Interestingly, the homologous relationship between pure Si and pure Ge is much stronger than that between pure Si and the $Si_{0.92}Ge_{0.08}$ alloy. This behavior is probably a result of the confined environment of the Ge atoms on the Si host lattice.[42] From the analysis of the mean static displacements it is clear that the volume occupied by the Ge atoms is larger than the average lattice spacing, hence the expansion of the lattice around

TABLE I. Observed phonon energies in the $Si_{0.92}Ge_{0.08}$ alloy.

q_x	q_y	q_z	E (meV)
	a(units of $2\pi/a$)		
	TA[110]		Σ_3
0.16	0.16	0.00	9.000±0.39
0.39	0.39	0.00	20.00±0.48
0.47	0.47	0.00	23.00±0.45
0.60	0.60	0.00	25.98±0.81
0.75	0.75	0.00	26.50±0.94
0.85	0.85	0.00	23.04±1.17
1.00	1.00	0.00	17.60±1.39
	LA[110]		Σ_1
0.10	0.10	0.00	9.000±0.32
0.20	0.20	0.00	18.00±0.35
0.32	0.32	0.00	26.00±0.47
0.43	0.43	0.00	31.00±0.78
0.50	0.50	0.00	34.48±1.18
0.60	0.60	0.00	38.69±0.87
0.70	0.70	0.00	42.96±0.62
0.80	0.80	0.00	46.12±0.53
1.00	1.00	0.00	50.28±0.72
	TA_1[111]		Λ_3
0.20	0.20	0.20	10.37±0.60
0.25	0.25	0.25	11.58±0.80
0.30	0.30	0.30	12.56±0.92
0.40	0.40	0.40	13.25±1.13
0.50	0.50	0.50	13.37±1.29
	LA[111]		Λ_1
0.10	0.10	0.10	12.00±0.54
0.20	0.20	0.20	22.00±0.66
0.30	0.30	0.30	32.00±0.95
0.40	0.40	0.04	40.30±1.06
	TA[001]		Δ_5
0.00	0.00	0.21	8.000±0.80
0.00	0.00	0.35	12.00±0.76
0.00	0.00	0.40	13.17±1.31
0.00	0.00	0.50	15.33±1.75
0.00	0.00	0.60	17.28±1.58
0.00	0.00	0.80	17.80±1.04
0.00	0.00	0.90	17.76±1.20
0.00	0.00	1.00	17.60±1.39
	LA[001]		Δ_1
0.00	0.00	0.10	6.000±0.49
0.00	0.00	0.14	9.000±0.46
0.00	0.00	0.20	12.00±0.36
0.00	0.00	0.29	18.00±0.51
0.00	0.00	0.41	24.00±0.57
0.00	0.00	0.51	30.00±0.55
0.00	0.00	0.58	34.00±0.59
0.00	0.00	0.79	42.00±1.99
0.00	0.00	1.00	50.28±0.72

them. This will stiffen the force constants between the Ge-Si and Ge-Ge pairs and thereby increase the phonon energies. In addition, the nonideal local atomic environments will affect the electronic structure and will, in general, cause Eq. (10) to be less valid. The manner in which these effects occur requires further study.

Additional transverse modes were observed close to the zone boundary in the [001] direction. Curiously, these extra modes lie near the TA[001] branch of pure Ge (see Fig. 3). In dilute alloys the minority atomic species can be treated as substitutional defects in the host lattice. If the solute atoms have the greater mass, in-band (or resonance) modes are often observed. We believe the additional TA[001] modes to be of this type and they may be responsible for the increased width of the phonon groups observed in the Δ_1 and Δ_5 directions as evidenced by the size of the error bars in Fig. 3. Resonance modes have also been reported in alloys of Cu(Au),[43] Cr(W),[44] Ni(Pt),[45] Al(Ag),[46] Y(Tb),[47] Mo(Re),[48] and Ni(Pd).[49] Theories that only consider mass disorder[50,51] (i.e., they assume that the force constants do not depend on the local atomic environment in the crystal) are capable of explaining the presence of resonance modes. This coherent-potential approximation seems to predict accurately both the position and the width of the resonance modes we observe in the Si-Ge alloy. However, here as well as with the majority of the other reported instances of resonance modes, it appears that force-constant disorder needs to be included in the theory. In particular, is seems difficult to reproduce the strong intensity of the phonon groups associated with the in-band modes using a simple low-concentration mass defect theory. The phonon energies of the local modes (which occur when a light atom is placed on a lattice of heavier atoms) observed in a $Ge_{0.908}Si_{0.092}$ single crystal were reported to exhibit a dependence on **Q**, contrary to the prediction of the isolated-defect theory.[52] We could not discern any dependence on **Q** for the resonance modes observed here and it is not clear from current theory what the dependence should be. As noted earlier, these modes do seem to occur at the same energies as in pure Ge, albeit considerably broadened, as are the phonon groups of the alloy at these wave vectors, suggesting a strong interference.

V. CONCLUSION

In conclusion, no atomic short-range order was observed in either of the crystals. The most probable explanation for this is that the effective equilibrium temperature is too close to the melting temperature to observe any ordering or clustering tendencies. Crystals with lower effective equilibrium temperatures are needed to study the formation of concentration fluctuations in the alloy. It is possible that this can be achieved by (neutron) irradiating the crystals to enhance the atomic diffusion while annealing at a lower temperature. Diffuse scattering arising from the static displacements was observed and the lattice was found to be expanded in the vicinity of the stronger scatterer, Ge. However, little quantitative information could be obtained without the complete set of data required to extract the species-dependent static displacements. Future experiments are planned to address these issues.

The phonon dispersion was found to be very similar to that of pure Si. The phonon energies were, however, found to be consistently higher than expected from the homologous relationship between pure Si and pure Ge. This behavior is most likely due to the confined local atomic environment of the Ge atoms on the Si host lattice, resulting in stiffer force constants. Additional transverse modes were observed in the [001] direction near the energy for the Δ_5=TA[001] branch of pure Ge and are attributed to resonance modes. X-ray synchrotron measurements of the optic phonons are planned for beamline ID16 at the European Synchrotron Research Facility. These measurements will provide more insight into the effect of alloying on the force constants.

ACKNOWLEDGMENTS

The authors would like to thank H. G. Smith, R. M. Nicklow, and B. Fultz for their extremely insightful comments on the nature of the phonon dispersion in disordered alloys. The portion of this work conducted at the University of Houston was supported by the NSF under Grant No. DMR 9729297. D.B. was also on partial support from the Texas Center of Superconductivity at the University of Houston. H.R. was supported by the Alexander von Humbolt Foundation during his tenure at the University of Houston and is currently supported by the Max Planck Institute für Metallforschung in Stuttgart. ORNL is managed by Lockheed Martin Energy Research Corp. under Contract No. DE-AC05-96OR22464 for the DOE. The NSLS at BNL is supported by the DOE through the Division of Materials and Chemical Sciences.

*Present address: European Synchrotron Radiation Facility, Boîte Postale 220, F-38043 Grenoble, France.

[1] B. S. Meyerson, Sci. Am. **270**, 62 (1994).
[2] F. Schaffler, Semicond. Sci. Technol. **12**, 1515 (1997).
[3] D. J. Paul, Adv. Mater. **11**, 191 (1999).
[4] K. Said, J. Poortmans, M. Caymax, R. Loo, A. Dami, G. Bremond, O. Kruger, and M. Kittler, Thin Solid Films **337**, 85 (1999).
[5] J. H. Li, C. S. Peng, Z. H. Mai, J. M. Zhou, Q. Huang, and D. Y. Dai, J. Appl. Phys. **86**, 1292 (1999).
[6] P. M. Mooney, F. K. LeGoues, J. Tersoff, and J. O. Chu, J. Appl. Phys. **75**, 3968 (1994).
[7] G. Bauer, J. Li, and E. Koppensteiner, J. Cryst. Growth **157**, 61 (1995).
[8] M. J. Shaw, P. R. Briddon, and M. Jaros, Thin Solid Films **294**, 166 (1997).
[9] S. Satpathy, R. M. Martin, and C. G. Van de Walle, Phys. Rev. B **38**, 13 237 (1988).
[10] B. S. Meyerson, Proc. IEEE **80**, 1592 (1992).
[11] E. Kasper, H. J. Herzog, and H. Kibbel, Appl. Phys. Lett. **8**, 199 (1975).
[12] R. People, IEEE J. Quantum Electron. **QE22**, 1696 (1986).

[13] D. Rosenfeld and S. A. Alterovitz, Solid-State Electron. **37**, 119 (1994).
[14] P. M. Mooney, F. K. LeGoues, and J. L. Jordan-Sweet, Appl. Phys. Lett. **65**, 2845 (1994).
[15] F. Liu and M. G. Lagally, Surf. Sci. **386**, 169 (1997).
[16] N. V. Abrosimov, S. N. Rossolenko, W. Thieme, A. Gerhardt, and W. Schröder, J. Cryst. Growth **174**, 182 (1997); N. V. Abrosimov, S. N. Rossolenko, V. Alex, A. Gerhardt, and W. Schröder, *ibid.* **166**, 657 (1996).
[17] D. Bliss, B. Demczyk, A. Anselmo, and J. Bailey, J. Cryst. Growth **174**, 187 (1997).
[18] H. P. Klug and L. E. Alexander, *X-ray Diffraction Procedures for Polycrystalline and Amorphous Materials* (Wiley, New York, 1974).
[19] H. Stohr and W. Klemm, Z. Anorg. Allg. Chem. **241**, 313 (1939).
[20] J. P. Dismukes, L. Ekstron, and R. J. Paff, J. Phys. Chem. **68**, 3021 (1964).
[21] A. Qteish and R. Resta, Phys. Rev. B **37**, 6983 (1988).
[22] P. C. Kelires and J. Tersoff, Phys. Rev. Lett. **63**, 1164 (1989).
[23] S. De Gironcoli, P. Giannozzi, and S. Baroni, Phys. Rev. Lett. **66**, 2116 (1991).
[24] G. Garbulsky, Ph.D. thesis, Massachusetts Institute of Technology (1996).
[25] Ya. S. Umanskii, V. I. Prilepskii, and S. S. Gorelik, Fiz. Tverd. Tela (Leningrad) **7**, 2673 (1965) [Sov. Phys. Solid State **7**, 2162 (1966)].
[26] H. Reichert, S. C. Moss, P. Imperatori, and K. Evans-Lutterodt, Appl. Phys. Lett. **74**, 531 (1999).
[27] J. Z. Tischler, J. D. Budai, D. E. Jesson, G. Eres, P. Zschack, J.-M. Baribeau, and D. C. Houghton, Phys. Rev. Lett. **68**, 2062 (1992).
[28] T. Araki, N. Fujimura, T. Ito, A. Wakahara, and A. Sasaki, J. Appl. Phys. **80**, 3804 (1996); T. Araki, N. Fijimura, and T. Ito, J. Cryst. Growth **174**, 675 (1997).
[29] S. Minomura, K. Tsuji, M. Wakagi, T. Ishidate, K. Inoue, and M. Shibuya, J. Non-Cryst. Solids **59**, 541 (1983).
[30] B. Borie and C. J. Sparks, Acta Crystallogr., Sect. A: Cryst. Phys., Diffr., Theor. Gen. Crystallogr. **27**, 198 (1971).
[31] X. Jiang, G. E. Ice, C. J. Sparks, J. L. Robertson, and P. Zschack, Phys. Rev. B **54**, 3211 (1996).
[32] L. Reinhard, J. L. Robertson, S. C. Moss, G. E. Ice, P. Zschack, and C. J. Sparks, Phys. Rev. B **45**, 2662 (1992).
[33] D. Le Bolloc'h, R. Caudron, and A. Finel, Phys. Rev. B **57**, 2801 (1998).
[34] S. Froyen and C. Herring, J. Appl. Phys. **52**, 7165 (1981).
[35] G. Nilsson and G. Nelin, Phys. Rev. B **6**, 3777 (1972).
[36] T. I. Kucher, Fiz. Tverd. Tela (Leningrad) **4**, 2385 (1962) [Sov. Phys. Solid State **4**, 1747 (1963)].
[37] W. Cochran, Proc. R. Soc. London, Ser. A **253**, 260 (1959).
[38] K. B. Tolpygo, Fiz. Tverd. Tela (Leningrad) **3**, 943 (1961) [Sov. Phys. Solid State **3**, 685 (1961)].
[39] G. Dolling, *Inelastic Scattering of Neutrons in Solids and Liquids* (International Atomic Energy Agency, Vienna, 1963), Vol. II, p. 37.
[40] B. N. Brockhouse and P. K. Iyengar, Phys. Rev. **111**, 747 (1958).
[41] G. Nilsson and G. Nelin, Phys. Rev. B **3**, 364 (1971).
[42] P. D. Bogdanoff and B. Fultz, Philos. Mag. B **79**, 753 (1999).
[43] E. C. Svensson and B. N. Brockhouse, Phys. Rev. Lett. **18**, 858 (1967); Solid State Commun. **3**, 245 (1965).
[44] R. M. Cinningham, L. D. Muhlestein, W. M. Shaw, and C. W. Tompson, Phys. Rev. B **2**, 4864 (1970); H. B. Moller and A. R. Mackintosh, Phys. Rev. Lett. **15**, 623 (1965).
[45] N. Kunitomi, Y. Tsunoda, and Y. Hiraga, Solid State Commun. **13**, 495 (1973); Y. Tsunoda, N. Kunitomi, N. Wakabayashi, R. M. Nicklow, and H. G. Smith, Phys. Rev. B **19**, 2876 (1979).
[46] A. Zinken, U. Buchenau, H. J. Fenzl, and H. R. Schober, Solid State Commun. **22**, 693 (1977).
[47] M. Mostoller, T. Kaplan, N. Wakabayashi, and R. M. Nicklow, Phys. Rev. B **10**, 3144 (1974).
[48] H. G. Smith, N. Wakabayashi, and M. Mostoller, in *Superconductivity in d- and f-Band Metals*, edited by D. H. Douglas (Plenum, New York, 1972), p. 223.
[49] W. A. Kamitakahara and B. N. Brockhouse, Phys. Rev. B **10**, 1200 (1974).
[50] R. J. Elliot and D. W. Taylor, Proc. R. Soc. London, Ser. A **296**, 161 (1967).
[51] D. W. Taylor, Phys. Rev. **156**, 1017 (1967).
[52] N. Wakabayashi, Phys. Rev. B **8**, 6015 (1973); N. Wakabayashi, R. M. Nicklow, and H. G. Smith, *ibid.* **4**, 2558 (1971).